

# DEEP UZAWA FOR PDE CONSTRAINED OPTIMISATION

CHARALAMBOS G. MAKRIDAKIS, AARON PIM, AND TRISTAN PRYER

**ABSTRACT.** In this work, we present a numerical solver for optimal control problems constrained by linear and semi-linear second-order elliptic PDEs. The approach is based on recasting the problem and includes an extension of Uzawa’s algorithm to build approximating sequences for these constrained optimal control problems. We prove strong convergence of the iterative scheme in their respective norms, and this convergence is generalised to a class of restricted function spaces. We showcase the algorithm by demonstrating its use numerically with neural network methods that we coin Deep Uzawa Algorithms and show they perform favourably compared with some existing Deep Neural Network approaches.

## 1. INTRODUCTION

Optimal control problems subject to physical constraints such as partial differential equations (PDEs) represent an important class of problems in both science and engineering. These problems have applications in various domains, such as fluid flow [12], heat conduction [16], structural optimisation [18], crystal growth [8] and radiotherapy [10], to name just a few. The ability to quickly and accurately model and solve these problems is important for advancements in these fields.

The mathematical theory of distributed and boundary optimal control problems subject to linear and nonlinear, elliptic and parabolic PDEs is well established, providing a robust theoretical foundation for addressing these challenges [4, 24, 11]. Numerically, common approaches to solving these problems involve formulating first-order optimality systems, which typically introduce either adjoint states or Lagrange multipliers. These formulations help in deriving the necessary conditions for optimality and form the basis for various numerical algorithms.

The continuous formulations of these optimal control problems are often discretised using finite element methods [1, 5], spectral methods [25] or wavelet methods [19]. Finite element methods are widely used due to their flexibility in handling complex geometries and boundary conditions, while spectral methods are preferred for their high accuracy in solving problems with smooth solutions. Wavelet methods are employed because they offer a multi-resolution analysis, which can efficiently capture localised features and singularities in the solution. All three methods transform the continuous problem into a discrete one, which can then be tackled using established optimisation algorithms such as gradient descent, semismooth Newton methods and the alternating direction method of multipliers [9, 3]. The choice of discretisation method often depends on the specific characteristics of the problem at hand, such as the nature of the domain, the smoothness of the solution, and the computational resources available.

In practical implementation, these discretised formulations are iteratively solved to update the control variables, ensuring convergence to an optimal solution. Despite the effectiveness of these traditional numerical methods, they can be computationally intensive, particularly for high-dimensional problems or those with complex constraints. This has led to the exploration of novel approaches, including the integration of deep neural networks, to improve computational efficiency and accuracy in solving PDE-constrained optimal control problems [20, 2, 26, 21]. For instance, physics-informed neural networks (PINNs) [23] have been adapted to enforce hard constraints in challenging topology optimisation problems, showing promise in handling the high dimensionality and PDE constraints characteristic of such inverse design problems [20]. In [2, 26, 21], two primary classes of methods have emerged: penalty-based methods and adjoint-based methods. Penalty methods transform the PDE-constrained optimisation problem into an unconstrained one by introducing an augmented loss function that includes the PDE residual. However, large penalty weights, necessary for enforcing PDE constraints accurately, can make the optimisation problem ill-conditioned and the choice of these weightings is not clear a priori. Adjoint-based methods on the other hand solve the adjoint

state equation to compute the derivative of the Lagrangian with respect to the control variable, iteratively updating the control.

The nature of the PDE constraint is also important. We illustrate our approach for a classical linear constraint, but nonlinear constraints are important in applications [6, 13, 22]. For example rigorous understanding of semilinear Allen-Cahn type constraints are challenging and the topic of ongoing research [7]. We give some numerical experiments to demonstrate our method is also applicable to a stationary Allen-Cahn equation.

In this work, we extend Uzawa’s algorithm [27] to develop approximating sequences for PDE-constrained optimal control problems using neural networks, introducing the Deep Uzawa Algorithms. Uzawa methods are a well known class of algorithm that generate iterative approximations for saddle point problems, [27, 9]. Standard convergence proofs [9] impose severe restrictions on mesh parameters when applied to PDE-constrained optimisation problems. The algorithm performs better with augmented Lagrangians, but it is still not the preferred method when using finite elements or other traditional PDE discretisation approaches. This is likely due to the appearance of high-order gradients in the optimality conditions. However, neural networks offer an alternative to discretisation with characteristics different from typical finite elements, being naturally suited to minimise energy functionals.

Our approach is to frame PDE-constrained optimisation problems in a functional analytic context where the Uzawa algorithm is fundamentally applicable. We design the resulting energies to inherently possess strong coercivity properties. Consequently, the resulting *deep Uzawa* neural network algorithms become highly efficient and robust. A key feature of our approach is the direct updating of the adjoint state within the iterative scheme, eliminating the need for an additional network for the adjoint variable. This makes our method computationally competitive with penalty-based approaches. As an initial step towards comprehensive convergence analysis, we provide rigorous mathematical proofs demonstrating the convergence of our iterative scheme at the PDE level (assuming exact solutions for the PDEs and energy minimisation problems) within their respective norms, and we further generalise this convergence to restricted function spaces. In forthcoming work, we will extend our analysis to account for errors due to neural network approximations.

To validate the practical utility of our approach, we present numerical examples that extend our method to semi-linear PDE constraints. This work represents an advancement in the integration of neural network architectures with traditional optimisation techniques, offering a robust and efficient solution framework for complex optimal control problems.

The remainder of the paper is structured as follows: In §2 we introduce the PDE constrained optimisation framework, we explore appropriate modifications of the underlying Lagrangian and in §3 we state the main results of this contribution. In §4 we introduce the neural network approximation and the Deep Uzawa method. In §5 we illustrate various numerical experiments with linear constraints, extending these experiments to semi-linear constraints in §6. Finally, §7 concludes the paper with the formal proofs of the main theorems.

## 2. PROBLEM SETTING AND APPROACH

**2.1. Model PDE Constrained Optimisation.** Let  $\Omega \subset \mathbb{R}^d$  be a bounded, convex domain. Throughout this work we denote the standard Lebesgue spaces by  $L^p(\omega)$ ,  $1 \leq p \leq \infty$ ,  $\omega \subset \mathbb{R}^d$ ,  $d = 1, 2, 3$ , with corresponding norms  $\|\cdot\|_{L^p(\omega)}$ . In the case  $p = 2$ , we use  $\|\cdot\|$  and  $\langle \cdot, \cdot \rangle$  to denote the norm and inner product, respectively. We then introduce the Sobolev spaces [14]

$$(2.1) \quad \mathbf{H}^k(\Omega) := \{ \phi \in L^2(\Omega) : D^\alpha \phi \in L^2(\Omega), \text{ for } |\alpha| \leq k \},$$

which are equipped with norms and semi-norms

$$(2.2) \quad \|u\|_{\mathbf{H}^k(\Omega)}^2 := \sum_{|\alpha| \leq k} \|D^\alpha u\|_{L^2(\Omega)}^2 \quad \text{and} \quad |u|_k^2 := |u|_{\mathbf{H}^k(\Omega)}^2 = \sum_{|\alpha|=k} \|D^\alpha u\|_{L^2(\Omega)}^2$$

respectively, where  $\alpha = \{\alpha_1, \dots, \alpha_d\}$  is a multi-index,  $|\alpha| = \sum_{i=1}^d \alpha_i$  and derivatives  $D^\alpha$  are understood in a weak sense.

Optimal control problems constrained by PDEs involve finding a control function that minimises a given cost functional while satisfying a PDE constraint. To that end, let  $\mathbf{H}(\Omega) := \mathbf{H}^2(\Omega) \cap \mathbf{H}_0^1(\Omega)$  and

$$(2.3) \quad K : \mathbf{H}(\Omega) \times \mathbf{L}^2(\Omega) \rightarrow \mathbf{L}^2(\Omega)$$

denote the residual of a second order PDE.

For a cost functional  $\widehat{J} : \mathbf{H}(\Omega) \times \mathbf{L}^2(\Omega) \rightarrow \mathbb{R}$ , the constrained minimisation problem is to find

$$(2.4) \quad \begin{aligned} (u^*, f^*) &= \arg \min_{u, f \in \mathbf{H}(\Omega) \times \mathbf{L}^2(\Omega)} \widehat{J}(u, f) \\ &\text{subject to } K(u, f) = 0 \text{ in } \Omega, \end{aligned}$$

where  $u$  is the state variable and  $f$  is the control variable. Let

$$(2.5) \quad \mathbf{L}_0^2(\Omega) := \{ \phi \in (\mathbf{L}^2 \cap \mathbf{BV})(\Omega) : \phi(x) = 0, \forall x \in \partial\Omega \}.$$

One approach to solving the above problem is to introduce a Lagrangian,  $\widehat{L} : \mathbf{H}(\Omega) \times \mathbf{L}^2(\Omega) \times \mathbf{L}_0^2(\Omega) \rightarrow \mathbb{R}$ , where the constraint is imposed via a Lagrange multiplier  $z \in \mathbf{L}_0^2(\Omega)$ . The Lagrangian is defined as

$$(2.6) \quad \widehat{L}(u, f, z) := \widehat{J}(u, f) + \langle K(u, f), z \rangle.$$

This gives rise to a saddle point problem whereby (2.4) is equivalent to finding

$$(2.7) \quad (u^*, f^*, z^*) = \arg \min_{u, f \in \mathbf{H}(\Omega) \times \mathbf{L}^2(\Omega)} \arg \max_{z \in \mathbf{L}_0^2(\Omega)} \widehat{L}(u, f, z).$$

The optimal solution can be determined through the first-order optimality conditions, which are computed by examining where the Fréchet derivative of the Lagrangian vanishes, that is,

$$(2.8) \quad D\widehat{L}(u, f, z) = \begin{bmatrix} \widehat{L}_u(u, f, z) \\ \widehat{L}_f(u, f, z) \\ \widehat{L}_z(u, f, z) \end{bmatrix} = \begin{bmatrix} \widehat{J}_u(u, f) + \langle K_u(u, f), z \rangle \\ \widehat{J}_f(u, f) + \langle K_f(u, f), z \rangle \\ K(u, f) \end{bmatrix} = \mathbf{0}.$$

Most traditional methods solve the above system of equations by employing various PDE discretisation methods. It is apparent that it is indeed computationally challenging to solve this fully coupled system, especially in high-dimensional problems or when the PDE constraint is time-dependent.

To illustrate the main idea behind our approach, we consider a simple linear-quadratic PDE-constrained optimisation problem. Note however that our approach can be extended to much more involved problems. Let the cost functional  $\widehat{J}$  be defined as

$$(2.9) \quad \widehat{J}(u, f) := \frac{1}{2} \|u - \mathcal{D}\|_{\mathbf{L}^2(\Omega)}^2 + \frac{\alpha}{2} \|f\|_{\mathbf{L}^2(\Omega)}^2,$$

where  $\mathcal{D}$  is the target state, and  $\alpha > 0$  is a regularisation parameter. The PDE constraint is given by

$$(2.10) \quad K(u, f) := \Delta u + f = 0 \text{ in } \Omega,$$

with zero Dirichlet boundary conditions. The Lagrangian functional corresponding to this problem is

$$(2.11) \quad \widehat{L}(u, f, z) = \frac{1}{2} \|u - \mathcal{D}\|_{\mathbf{L}^2(\Omega)}^2 + \frac{\alpha}{2} \|f\|_{\mathbf{L}^2(\Omega)}^2 - \langle K(u, f), z \rangle.$$

Computing the Fréchet derivatives of  $\widehat{L}$  with respect to  $u$ ,  $f$ , and  $z$ , we obtain the system

$$(2.12) \quad \begin{aligned} -\Delta z + u &= \mathcal{D} \\ \alpha f - z &= 0 \\ -\Delta u - f &= 0 \end{aligned}$$

This system represents the first-order optimality conditions for the PDE-constrained optimisation problem. The optimal solution  $(u^*, f^*, z^*) \in \mathbf{H}(\Omega) \times \mathbf{L}^2(\Omega) \times \mathbf{L}_0^2(\Omega)$  determines a saddle point of the Lagrangian.

**2.2. A strongly coercive Lagrangian.** A key observation is that, although the optimality conditions (2.12) is a well posed PDE system, rarely one solves it using direct methods, see e.g. [24], for the finite element case. As mentioned, a particular attractive iterative method at the PDE level is Uzawa, which produces iterates,

$$(2.13) \quad \begin{aligned} (u^k, f^k) &= \arg \min_{u, f \in \mathbf{H}(\Omega) \times \mathbf{L}^2(\Omega)} \widehat{L}(u, f, z^k) \\ z^{k+1} &= z^k + \rho K(u^k, f^k), \end{aligned}$$

see Section 2.3 for precise definitions.

The primary advantage of (2.13) is that each iteration involves solving a minimisation problem, and the Lagrange multiplier is updated straightforwardly. This formulation is particularly well-suited for neural network approximations. However, when finite elements are used, the algorithm's stability is known to be guaranteed only under strict mesh restrictions. Furthermore, for neural networks, methods based on (2.13), we have observed that the scheme exhibits computational instability; we refer to the next section for detailed formulations of neural network approximations.

To address this issue, we introduce the modified functional

$$(2.14) \quad J(u, f) := \frac{1}{2} \|u - \mathcal{D}\|_{\mathbf{L}^2(\Omega)}^2 + \frac{\alpha}{4} \|f\|_{\mathbf{L}^2(\Omega)}^2 + \frac{\alpha}{4} \|\Delta u\|_{\mathbf{L}^2(\Omega)}^2,$$

and seek

$$(2.15) \quad (u^*, f^*) = \arg \min_{u, f \in \mathbf{H}(\Omega) \times \mathbf{L}^2(\Omega)} J(u, f)$$

subject to the constraint

$$(2.16) \quad K(u, f) = 0 \text{ in } \Omega.$$

The modification to the cost functional  $J(u, f)$  includes a consistent regularisation term  $\frac{\alpha}{4} \|\Delta u\|_{\mathbf{L}^2(\Omega)}^2$ , which helps to balance the relative strength of the functional with the regularity requirements imposed by the PDE constraint. This regularisation term is important in ensuring the well-posedness of the optimisation problem and improving the convergence properties of the iterative solution methods.

The solution to the modified problem is equivalent to the solution to the minimisation problem, given in equation (2.9), which may be seen by comparing the first-order optimality conditions of each problem. Indeed, let us define

$$(2.17) \quad L(u, f, z) := J(u, f) + \langle K(u, f), z \rangle.$$

The first-order optimality conditions are

$$(2.18) \quad DL(u, f, z) = \begin{bmatrix} L_u(u, f, z) \\ L_f(u, f, z) \\ L_z(u, f, z) \end{bmatrix} = \begin{bmatrix} J_u(u, f) + \langle K_u(u, f), z \rangle \\ J_f(u, f) + \langle K_f(u, f), z \rangle \\ K(u, f) \end{bmatrix} = \mathbf{0}.$$

These conditions yield

$$(2.19) \quad \begin{aligned} \frac{\alpha}{2} \Delta^2 u - \Delta z + u &= \mathcal{D} \\ \frac{\alpha}{2} f + z &= 0 \\ \Delta u + f &= 0. \end{aligned}$$

Unlike other approaches, we do not solve the KKT conditions explicitly, instead we examine the Lagrangian formulation directly. We seek the saddle points of the Lagrangian  $L$ , that satisfy  $(u^*, f^*, z^*) \in \mathbf{H}(\Omega) \times \mathbf{L}^2(\Omega) \times \mathbf{L}_0^2(\Omega)$  such that

$$(2.20) \quad (u^*, f^*, z^*) = \arg \min_{u, f \in \mathbf{H}(\Omega) \times \mathbf{L}^2(\Omega)} \arg \max_{z \in \mathbf{L}_0^2(\Omega)} L(u, f, z).$$

**2.3. Iterative Approximation.** To motivate our neural network methods introduced in the next section, we first define the iterates at the PDE level. We propose an iterative method for the solution of (2.7) through an Uzawa algorithm at the continuum. The Uzawa algorithm iteratively generates sequences of functions  $\{u^k\}_{k=0}^\infty \subset H(\Omega)$ ,  $\{f^k\}_{k=0}^\infty \subset L^2(\Omega)$ , and  $\{z^k\}_{k=0}^\infty \subset L_0^2(\Omega)$ . These are defined through an initial guess  $z^0 \in L_0^2(\Omega)$ . Then for a step size  $\rho > 0$  that will be specified, for  $k = 0, 1, 2, \dots$ , find  $u^k, f^k$  such that

$$(2.21) \quad \begin{aligned} (u^k, f^k) &= \arg \min_{u, f \in H(\Omega) \times L^2(\Omega)} L(u, f, z^k) \\ z^{k+1} &= z^k + \rho K(u^k, f^k). \end{aligned}$$

At each iteration, we first solve a minimisation problem that can be quantified through the first-order optimality conditions:

$$(2.22) \quad \begin{aligned} \frac{\alpha}{2} \Delta^2 u + u &= \mathcal{D} - \Delta z^k \\ f &= -\frac{2}{\alpha} z^k. \end{aligned}$$

We emphasise however that our intention is to discretise (2.21) directly, and not via the optimality conditions (2.22).

**2.4. Other Modified Lagrangian Approaches.** An issue in posing classical iterative approaches to the solution of (2.7) is the relative strength of the functional  $\hat{J}$  with respect to the regularity requirements of the PDE constraint. Classical methods for solving PDE-constrained optimisation problems include penalty methods, adjoint-based methods, and augmented Lagrangian methods. Penalty methods transform the constrained problem into an unconstrained one by adding a penalty term to the cost functional that enforces the PDE constraint. For example

$$(2.23) \quad \frac{1}{2} \|u - \mathcal{D}\|_{L^2(\Omega)}^2 + \frac{\alpha}{2} \|f\|_{L^2(\Omega)}^2 + \frac{\beta}{2} \|K(u, f)\|_{L^2(\Omega)}^2 \rightarrow \min.$$

While this approach is straightforward, it often leads to ill-conditioned optimisation problems, particularly when the penalty parameter is large, as required to accurately enforce the constraint.

Adjoint-based methods, on the other hand, involve solving the adjoint state equation to compute the gradient of the cost functional with respect to the control variables. This gradient is then used in gradient-based optimisation algorithms such as gradient descent or quasi-Newton methods. In the simplest case, such an iterative method might resemble a Gauss-Siedel approach. For fixed  $f^0$  find  $u^{k+1}$  such that

$$(2.24) \quad \begin{aligned} -\Delta u^{k+1} &= f^k \\ -\Delta z^{k+1} &= \mathcal{D} - u^{k+1} \\ f^{k+1} &= -\frac{1}{\alpha} z^{k+1}. \end{aligned}$$

Although effective, adjoint-based methods can be computationally expensive and slow to converge, especially for complex PDEs or large-scale problems.

Augmented Lagrangian methods combine the advantages of penalty methods and Lagrange multipliers by adding both penalty terms and Lagrange multipliers to the cost functional. This approach improves the conditioning of the optimisation problem compared to penalty methods alone but still requires careful tuning of parameters and can be computationally intensive.

The augmented Lagrangian for this problem is

$$(2.25) \quad \mathcal{L}_\beta(u, f, z) := \hat{J}(u, f) + \langle K(u, f), z \rangle + \frac{\beta}{2} \|K(u, f)\|_{L^2(\Omega)}^2.$$

**Remark 2.5** (Comparison to the augmented Lagrangian method). *While we do not use the formulation directly, it is informative to compare the KKT conditions (2.19) with those of the augmented Lagrangian method (2.25). They are given as*

$$(2.26) \quad \begin{aligned} \beta \Delta(\Delta u + f) + \Delta z + u &= \mathcal{D} \\ \beta(\Delta u + f) + \alpha f + z &= 0 \\ \Delta u + f &= 0. \end{aligned}$$

It is important to note that each KKT system (2.26), (2.19) and (2.12) are consistent with one another and, for this model problem assuming smoothness and compatible boundary conditions, the control and dual variable can be eliminated to show that the state equation satisfies

$$(2.27) \quad \alpha \Delta^2 u + u = \mathcal{D}.$$

**Remark 2.6** (Augmented Lagrangian and an Uzawa iteration). *The Euler-Lagrange equation arising from the Uzawa minimisation problem (2.21) can be easily written for the augmented Lagrangian method.*

Indeed, for an initial guess  $z^0$ , for  $k = 0, 1, 2, \dots$  find  $u^{k+1}, f^{k+1}$  such that

$$(2.28) \quad (u^{k+1}, f^{k+1}) = \arg \min_{u, f} \widehat{J}(u, f) + \langle K(u, f), z^k \rangle + \frac{\beta}{2} \|K(u, f)\|_{L^2(\Omega)}^2.$$

and update

$$(2.29) \quad z^{k+1} = z^k + \beta K(u^{k+1}, f^{k+1}).$$

Note that the state, control update is equivalent to solving the Euler-Lagrange equations

$$(2.30) \quad \begin{aligned} \beta \Delta(\Delta u + f) + u &= \mathcal{D} - \Delta z^k \\ \beta(\Delta u + f) + \alpha f &= -z^k. \end{aligned}$$

The augmented Lagrangian method combines the penalty term with the Lagrange multipliers, which requires careful tuning of the penalty parameters to balance constraint enforcement and problem conditioning.

Both iterative schemes (2.22) and (2.30) fit into the analytic framework we present, thereby providing a theoretical understanding on the convergence behaviour of this method observed in [20]. However, our focus in this work is on (2.21).

### 3. CONVERGENCE ANALYSIS

As a first step towards a complete convergence analysis, we demonstrate the convergence of our iterative scheme at the PDE level, assuming exact solutions for the PDEs and energy minimisation problems. We then generalise this convergence to restricted function spaces. In future work, we will extend our analysis to account for errors due to neural network approximations. Here, we present the convergence result, with the proof deferred to §7. The proofs are based on appropriate adaptations of classical arguments regarding the convergence of Uzawa algorithms, see [9].

**Theorem 3.1.** *Assume that  $\Omega \subset \mathbb{R}^d$  is a convex polygonal domain. Let the sequences  $\{u^k\}_{k=0}^\infty \subset H(\Omega)$  and  $\{f^k\}_{k=0}^\infty \subset L^2(\Omega)$  be generated through the iterative method (2.21). Suppose  $u^* \in H(\Omega)$  and  $f^* \in L^2(\Omega)$  are critical points of (2.20). Then, for  $\rho \in (0, \frac{\alpha}{2})$ , we have that*

$$(3.1) \quad u^k \rightarrow u^* \text{ in } H^2(\Omega), \quad f^k \rightarrow f^* \text{ in } L^2(\Omega).$$

**Remark 3.2** (Generalised elliptic operators). *The results presented hold for more general elliptic operators, indeed any second order elliptic problem admitting  $u \in H^2(\Omega)$  regularity results falls under the same framework. It can also be extended to those problems that only admit a weak solution, on a non-convex domain say, albeit one only expects convergence in  $H^1(\Omega)$ . It is interesting to note that the admissible values of  $\rho$  have no dependence on the regularity constant.*

**3.3. Non-negativity constraint.** We define a restricted function space

$$(3.2) \quad H(\Omega, \mathbb{R}^+) := \{\phi \in H(\Omega) : \phi \geq 0\}, \quad L_0^2(\Omega, \mathbb{R}^+) := \{\psi \in L_0^2 : \psi \geq 0\}$$

and consider the PDE constrained optimisation problem

$$(3.3) \quad (u^*, f^*) = \arg \min_{u, f \in H(\Omega)^+ \times L^2(\Omega, \mathbb{R}^+)} J(u, f)$$

subject to the constraint given in (2.16). This may be formulated as a constrained saddle-point problem,

$$(3.4) \quad u^*, f^*, z^* = \arg \min_{u, f \in H(\Omega, \mathbb{R}^+) \times L^2(\Omega, \mathbb{R}^+)} \arg \max_{z \in L_0^2(\Omega, \mathbb{R}^+)} L(u, f, z).$$

Similar to the unconstrained case, we may construct an iterative Uzawa scheme which is derived from the first order optimality conditions. Let  $P^+ : L^2(\Omega) \rightarrow L^2(\Omega, \mathbb{R}^+)$  be the canonical projection operator given by

$$(3.5) \quad P^+ \phi(\mathbf{x}) := \max \{ \phi(\mathbf{x}), 0 \} \quad \forall \mathbf{x} \in \Omega.$$

For an initial guess  $z^0 \in L_0^2(\Omega, \mathbb{R}^+)$  and step size  $\rho > 0$ , for  $k = 0, 1, 2, \dots$  we seek  $u^k, f^k$  such that

$$(3.6) \quad \begin{aligned} u^k, f^k &= \arg \min_{u, f \in \mathbf{H}(\Omega, \mathbb{R}^+) \times L^2(\Omega, \mathbb{R}^+)} L(u, f, z^k) \\ z^{k+1} &= P^+ (z^k + \rho K(u^k, f^k)). \end{aligned}$$

**Theorem 3.4.** *Let  $\Omega \subset \mathbb{R}^d$  be a convex polygonal domain. Let the sequences  $\{u^k\}_{k=0}^\infty \subset \mathbf{H}(\Omega, \mathbb{R}^+)$  and  $\{f^k\}_{k=0}^\infty \subset L^2(\Omega, \mathbb{R}^+)$  be generated through the iterative method (3.6). Suppose  $u^* \in \mathbf{H}(\Omega, \mathbb{R}^+)$  and  $f^* \in L^2(\Omega, \mathbb{R}^+)$  are critical points of (3.4). Then, for  $\rho \in (0, \frac{\alpha}{2})$ , we have that*

$$(3.7) \quad u^k \rightarrow u^* \text{ in } \mathbf{H}^2(\Omega), \quad f^k \rightarrow f^* \text{ in } L^2(\Omega).$$

#### 4. DEEP UZAWA ALGORITHM

This section outlines the methodology for constructing a neural network approximation scheme, demonstrated with a series of examples.

**4.1. Neural Network Function Approximation.** We consider approximations to the PDE constrained optimisation problem generated by neural networks. The structure described is for illustrative purposes, and our results are not dependent on specific neural network architectures. A deep neural network maps each point  $x \in \Omega$  to a value  $w_\theta(x) \in \mathbb{R}$  through the process

$$(4.1) \quad w_\theta(x) = \mathcal{C}_L(x) := C_L \circ \sigma \circ C_{L-1} \circ \dots \circ \sigma \circ C_1(x) \quad \forall x \in \Omega.$$

The mapping  $\mathcal{C}_L : \mathbb{R}^d \rightarrow \mathbb{R}^2$  in our application. This  $\mathcal{C}_L$  is a neural network with  $L$  layers and an activation function  $\sigma$ . To define  $w_\theta(x)$  for all  $x \in \Omega_D$ , we use the same  $\mathcal{C}_L$ , thus  $w_\theta(\cdot) = \mathcal{C}_L(\cdot)$ .

Each map  $\mathcal{C}_L$  is characterised by intermediate (hidden) layers  $C_k$ , which are affine transformations of the form

$$(4.2) \quad C_k y = W_k y + b_k, \quad \text{where } W_k \in \mathbb{R}^{d_{k+1} \times d_k}, b_k \in \mathbb{R}^{d_{k+1}}.$$

Here, the dimensions  $d_k$  can vary with each layer  $k$ , and  $\sigma(y)$  represents the vector with the same number of components as  $y$ , where  $\sigma(y)_i = \sigma(y_i)$ . The index  $\theta$  collectively represents all parameters of the network  $\mathcal{C}_L$ , namely  $W_k, b_k$ , for  $k = 1, \dots, L$ . The set of all networks  $\mathcal{C}_L$  with a given structure (fixed  $L, d_k, k = 1, \dots, L$ ) of the form (4.1)–(4.2) is called  $\mathcal{N}$ .

The total dimension (number of degrees of freedom) of  $\mathcal{N}$  is

$$(4.3) \quad \dim \mathcal{N} = \sum_{k=1}^L d_{k+1} (d_k + 1).$$

We define the space of functions as

$$(4.4) \quad \mathcal{V}_N = \{w_\theta : \Omega \rightarrow \mathbb{R}, \text{ where } w_\theta(x) = \mathcal{C}_L(x) \text{ for some } \mathcal{C}_L \in \mathcal{N}\}.$$

It is important to note that  $\mathcal{V}_N$  is not a linear space. We denote by

$$(4.5) \quad \Theta = \{\theta : w_\theta \in \mathcal{V}_N\}$$

and note that  $\Theta$  is a linear subspace of  $\mathbb{R}^{\dim \mathcal{N}}$ .

The Deep Uzawa algorithm minimises residual-type functionals over the discrete space  $\mathcal{V}_N$ .

**Definition 4.2** (Deep- $\mathcal{V}_N$  minimiser). *For fixed  $z^k$ , assume that the problem*

$$(4.6) \quad \min_{(u, f) \in \mathcal{V}_N} L(u, f, z^k)$$

*has a solution  $(u^*, f^*) \in \mathcal{V}_N$ . We call  $(u^*, f^*)$  a deep- $\mathcal{V}_N$  minimiser of  $L(\cdot, \cdot, z^k)$ .*

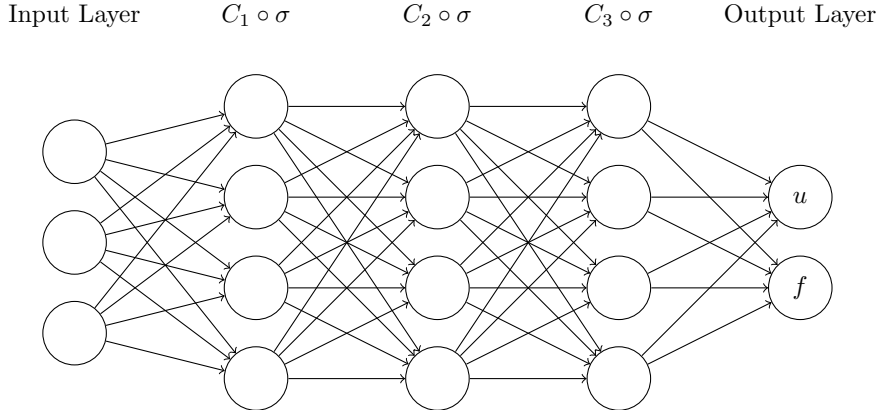


FIGURE 1. Illustration of the architecture within  $\mathcal{C}_L$ .

One key difficulty in this problem is that  $\mathcal{V}_N$  is not a linear space. Computationally, it can be equivalently formulated as a minimisation problem in  $\mathbb{R}^{\dim \mathcal{N}}$  by considering  $\theta$  as the parameter vector to be identified through

$$(4.7) \quad \min_{\theta \in \Theta} L(u_\theta, f_\theta, z^k).$$

Although this is well defined as a discrete minimisation problem, it is generally non-convex with respect to  $\theta$  even if the functional  $L(u, f, z)$  is convex with respect to  $(u, f)$  such as in the penalty methods. This is one of the primary technical challenges in machine learning algorithms.

**4.3. Training within the Deep Uzawa framework.** To implement the Deep Uzawa iteration, we need computable discrete versions of the Lagrangian  $L(u_\theta, f_\theta, z^k)$ . This can be achieved in different ways. A common approach is to use appropriate quadrature for integrals over  $\Omega$  (training through quadrature). To fix ideas, such a quadrature requires a set  $\mathcal{K}_h$  of discrete points  $y \in \mathcal{K}_h$  and corresponding nonnegative weights  $w_y$  such that

$$(4.8) \quad \sum_{y \in \mathcal{K}_h} w_y g(y) \approx \int_{\Omega_D} g(x) dx.$$

Then one can define the discrete functional

$$(4.9) \quad L_Q(u, f, z) = \sum_{y \in \mathcal{K}_h} w_y \left( \frac{1}{2} |u(y) - \mathcal{D}(y)|^2 + \frac{\alpha}{4} |f(y)|^2 + \frac{\alpha}{4} |\Delta u(y)|^2 + z(y) K(u(y), f(y)) \right).$$

Notice that both deterministic and probabilistic quadrature rules are possible, yielding different final algorithms.

In this work, we shall not consider in detail the influence of the quadrature (and hence of the training) on the stability and convergence of the algorithms. This requires a much more involved technical analysis and will be the subject of future research.

**4.4. The Deep Uzawa Iteration.** The Deep Uzawa algorithm combines the classical Uzawa iteration with neural network-based minimisation. This approach involves alternating between an inner loop consisting of several iterations of minimisation and an outer loop which corresponds to a single Uzawa update step as described in Algorithm 1. Note the total number of Epochs is the product  $N_{\text{SGD}} N_{\text{Uz}}$ .

## 5. NUMERICAL EXPERIMENTS: LINEAR CONSTRAINTS

We will now detail some numerical experiments. In each case we use the PyTorch Adam class optimiser [17] with learning rate  $\eta = 10^{-3}$ . Additionally, unless otherwise specified, we let  $N_{\text{SGD}} = 40$  and  $N_{\text{Uz}} = 500$ . Finally, we consider  $N = 201$  uniformly distributed collocation points that form a Cartesian grid, unless otherwise specified.

---

**Algorithm 1** Deep Uzawa Iteration
 

---

**Require:** Initial guess  $z^0 \in L_0^2(\Omega)$ , Uzawa step size  $\rho > 0$ , number of Uzawa steps  $N_{Uz}$ , number of Stochastic Gradient Descent iterations  $N_{SGD}$ , learning rate  $\eta$ .

- 1:  $k \leftarrow 0$
  - 2: Initialise neural network parameters  $\theta^0$
  - 3: **for**  $k = 0$  to  $N_{Uz} - 1$  **do**
  - 4:   **for**  $m = 0$  to  $N_{SGD} - 1$  **do**
  - 5:     Compute stochastic gradient  $\nabla_{\theta} L_Q(u_{\theta}^m, f_{\theta}^m, z^k)$
  - 6:     Update parameters:  $\theta^{m+1} \leftarrow \theta^m - \eta \nabla_{\theta} L_Q(u_{\theta}^m, f_{\theta}^m, z^k)$
  - 7:   **end for**
  - 8:    $(u^k, f^k) \leftarrow (u_{\theta}^{N_{SGD}}, f_{\theta}^{N_{SGD}})$
  - 9:   Update Lagrange multiplier:  $z^{k+1} \leftarrow z^k + \rho K(u^k, f^k)$
  - 10:    $k \leftarrow k + 1$
  - 11: **end for**
- 

5.1. **Example: Smooth Target.** To begin, we consider the one-dimensional interval  $\Omega = (0, 1)$  and target function

$$(5.1) \quad \mathcal{D}(x) = (1 + \alpha\pi^4) \sin(\pi x).$$

Here we compute

$$(5.2) \quad u^*(x, y) = \sin(\pi x), \quad f^*(x, y) = \pi^2 \sin(\pi x).$$

In Figure 2 we show the neural network approximation to both state and control, and the corresponding pointwise errors, for a particular choice of  $\alpha$ .

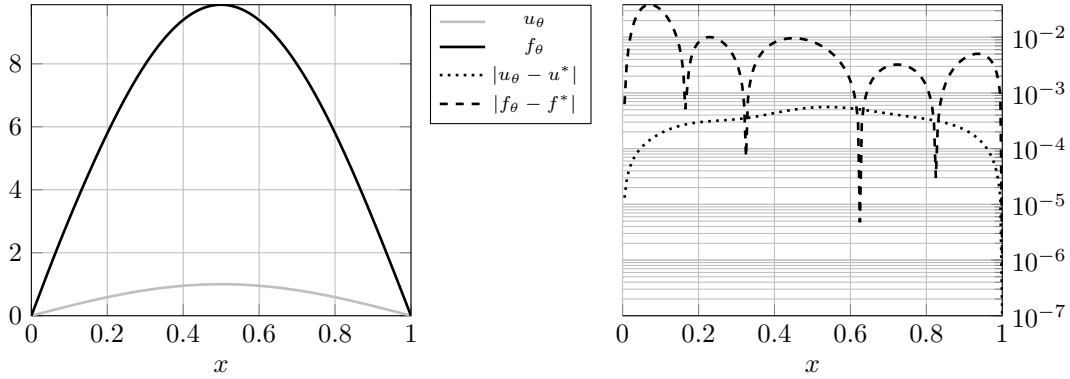


FIGURE 2. Example 5.1. Plots of the state and control (left), and the pointwise error (right), where the exact solutions  $u^*, f^* \in \mathcal{V}_N$  are given in equation (5.2), for  $\alpha = 10^{-4}$ .

In Figure 3 we show the  $L^2$ -error of the neural network approximation, for both state and control, against update number for varying  $\alpha$  values. The rate of convergence of the state, with respect to update number, is robust with respect to changes in  $\alpha$ . However, the rate of convergence of the control decreases, with respect to update number, as  $\alpha$  decreases. This is because the component of the loss functional that corresponds to the control is scaled with respect to  $\alpha$ .

In Figure 4 we show the  $L^2$ -error of the neural network approximation, for both state and control, against  $N_{Uz}$  for varying  $N_{SGD}$  values. This is quantifying the number of inner stochastic gradient descent iterations per Uzawa update.

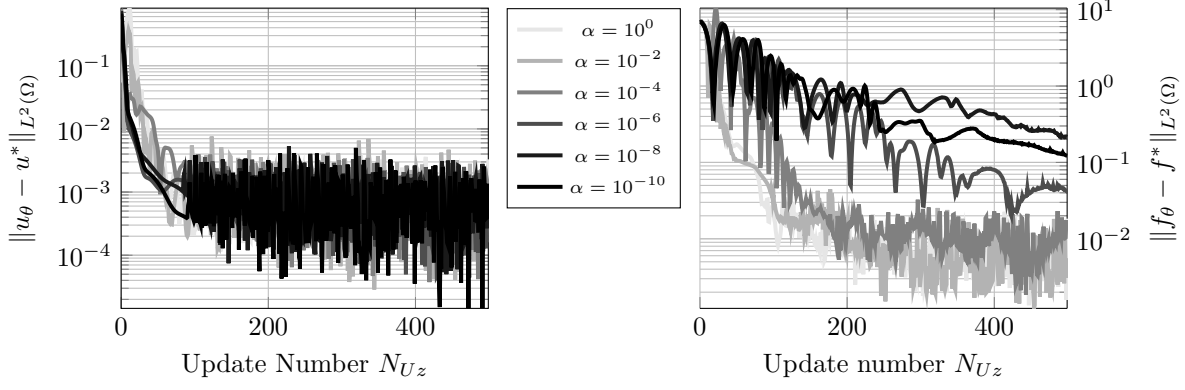


FIGURE 3. Example 5.1. Plots of the  $L^2$ -error of approximation of state and control as a function of  $N_{Uz}$  for various regularisations  $\alpha \in [10^{-10}, 1]$ .

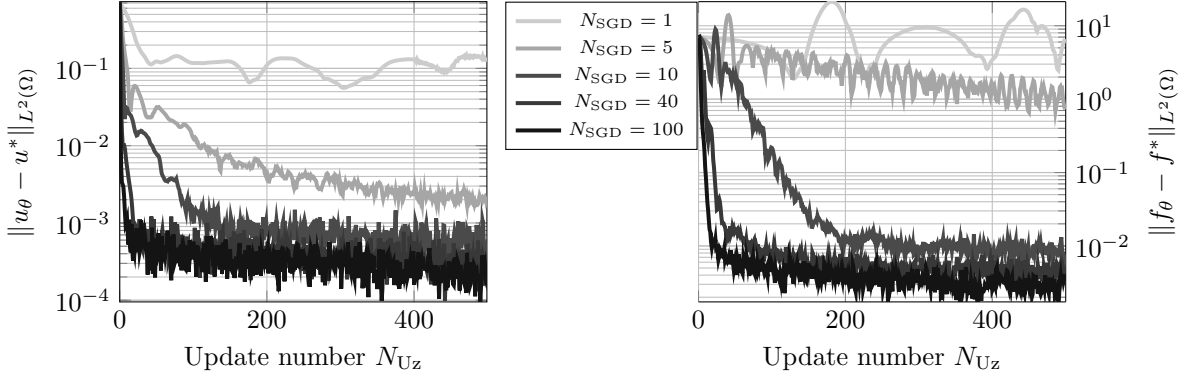


FIGURE 4. Example 5.1. Plots of the  $L^2$ -error of approximation of state and control for  $\alpha = 10^{-4}$  and  $N_{SGD} \in [1, 100]$ .

We compare our scheme to an augmented Lagrangian approach [20], equation (2.25). Recall the discrete functional  $L_Q$ , equation (4.9); for a given  $\beta > 0$  we define

$$(5.3) \quad \mathcal{L}_{\beta,Q}(u, f, z) = L_Q(u, f, z) + \frac{\beta}{2} \sum_{y \in \mathcal{K}_h} w_y (K(u(y), f(y)))^2.$$

Consider the following minimisation scheme:

$$(5.4) \quad \begin{aligned} (u_{\beta,\theta}^k, f_{\beta,\theta}^k) &= \arg \min_{u, f \in \mathcal{V}_N \times \mathcal{V}_N} \mathcal{L}_{\beta,Q}(u, f, z_{\beta,\theta}^k) \\ z_{\beta,\theta}^{k+1} &= z_{\beta,\theta}^k + \beta K(u_{\beta,\theta}^k, f_{\beta,\theta}^k). \end{aligned}$$

In Figure 5, we show the  $L^2$ -error of the neural network approximation of the augmented Lagrangian approach, for both state and control, against update number for varying  $\beta$  values and fixed  $\alpha = 10^{-4}$ . Note that the augmented Lagrangian approach performs comparably to the Deep Uzawa scheme for  $\beta \approx 10^{-4}$ .

**5.2. Example: Boundary Layers.** Again we take  $\Omega := (0, 1)$  but now  $\mathcal{D} = 1$ . As was observed in §2 the control can be eliminated from the KKT system and the optimal state satisfies

$$(5.5) \quad \begin{aligned} \alpha \Delta^2 u^* + u^* &= 1 \text{ in } \Omega \\ u^* &= \Delta u^* = 0 \text{ on } \partial\Omega. \end{aligned}$$

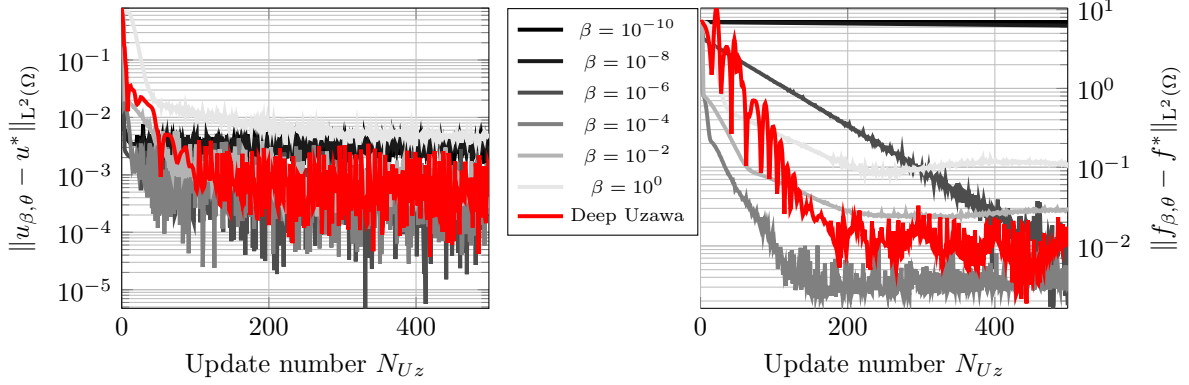


FIGURE 5. Example 5.1. lots of the  $L^2$ -error of augmented Lagrangian approximation of state and control  $u_{\beta,\theta}, f_{\beta,\theta} \in \mathcal{V}_N$ , equation (5.4) for  $\beta \in [10^{-10}, 1]$  and  $\alpha = 10^{-4}$ . The corresponding  $L^2$ -error between the Deep Uzawa state and control is plotted in red.

This problem induces boundary layers in the solution for small  $\alpha$ . One may write a closed form solution to this problem; let  $\omega := (4\alpha)^{-1/4}$  and  $y = \omega x$

(5.6)

$$u^*(x) = 1 - \cosh(y) \cos(y) + \frac{\sinh(\omega)}{\cosh(\omega) + \cos(\omega)} \sinh(y) \cos(y) - \frac{\sin(\omega)}{\cosh(\omega) + \cos(\omega)} \cosh(y) \sin(y)$$

$$f^*(x) = 2\omega^2 \left( \sinh(y) \sin(y) - \frac{\sinh(\omega)}{\cosh(\omega) + \cos(\omega)} \cosh(y) \sin(y) - \frac{\sin(\omega)}{\cosh(\omega) + \cos(\omega)} \sinh(y) \cos(y) \right).$$

An approximation to these functions is given in Figure 6

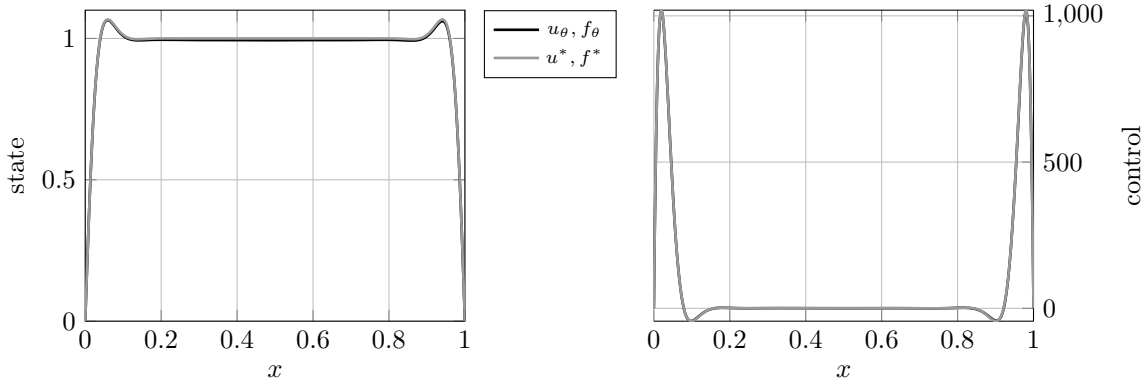


FIGURE 6. Example 5.2. Plots of the neural network approximation of the state and control and the exact solution, for  $\alpha = 10^{-7}$ .

In Figure 7, we observe that the average of pointwise error between the neural network approximations  $u_{\theta}, f_{\theta}$  increases as  $\alpha$  decreases. This is also observed in Figure 8, where we observe a smooth decrease in the rate of convergence of both the state and control, with respect to update number, as  $\alpha$  decreases.

In Figure 9, we plot the  $L^2$ -error of the neural network approximation to the state and control, against the update number  $N_{Uz}$ , and vary the number of stochastic gradient descent iterations  $N_{SDG}$ . In this figure

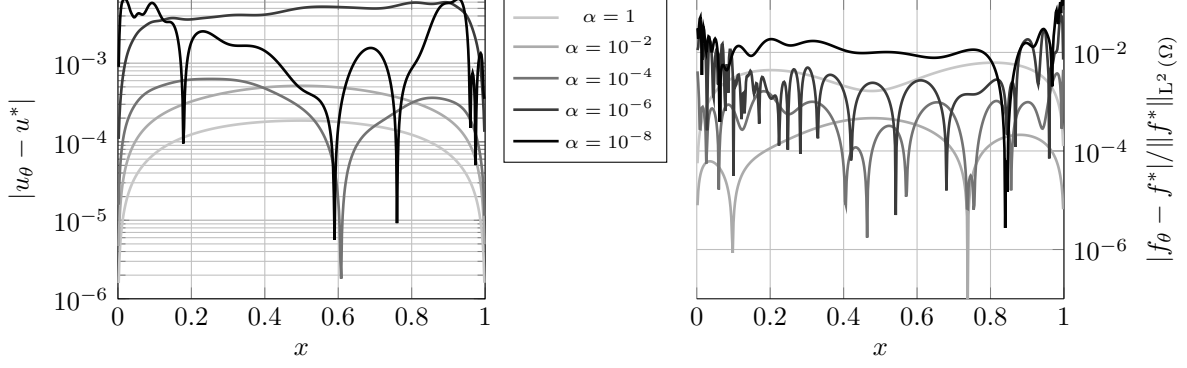


FIGURE 7. Example 5.2. Plots of the pointwise-error of the neural network approximation of the state and control, for  $\alpha \in [10^{-8}, 1]$ .

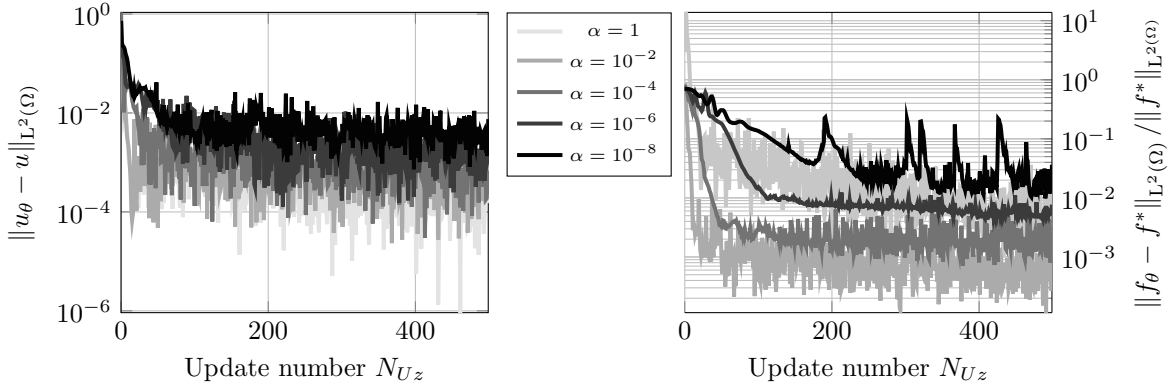


FIGURE 8. Example 5.2. Plots of the  $L^2$ -error of the neural network approximation of the state and control, for  $\alpha \in [10^{-8}, 1]$ .

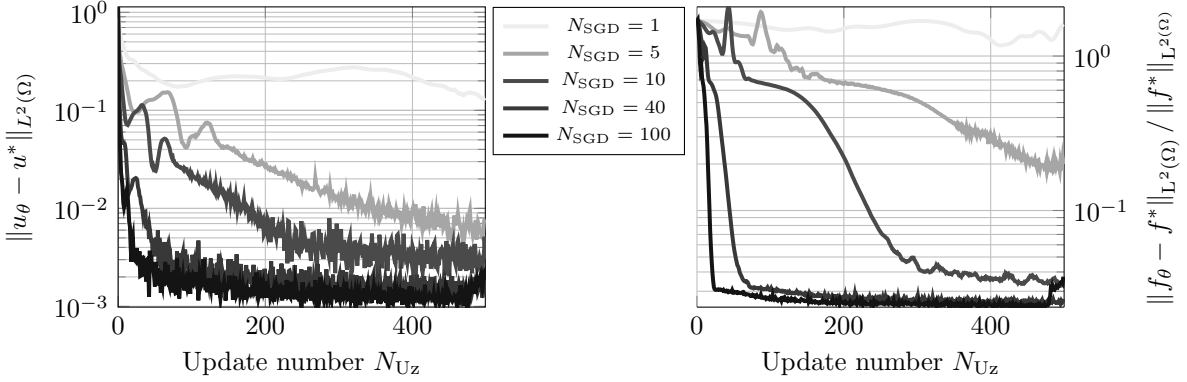


FIGURE 9. Example 5.2. Plots of the  $L^2$ -error of the neural network approximation of the state and control against update number  $N_{Uz}$  for  $\alpha = 10^{-5}$ , and  $N_{SGD} \in [1, 100]$ .

we observe that for small  $N_{SGD}$ , the error fails to converge with respect to the update number; for large  $N_{SGD}$ , the error for both the state and control converges.

5.3. **Example: 2d Smooth Target.** Consider the domain  $\Omega := (0, 1)^2$  and the target function  $\mathcal{D}$  is given by

$$(5.7) \quad \mathcal{D}(x) = (1 + 4\alpha\pi^4) \sin(\pi x) \sin(\pi y).$$

The optimal state and control is then

$$(5.8) \quad u^*(x, y) = \sin(\pi x) \sin(\pi y), \quad f^*(x, y) = 2\pi^2 \sin(\pi x) \sin(\pi y).$$

In Figure 10, we show a neural network approximation to the state and control as well as the pointwise error. Additionally, we have that for that control, the points of greatest error occur on the boundary.

In Figure 11, we examine the  $L^2(\Omega)$  errors for both state and control for various  $\alpha$ .

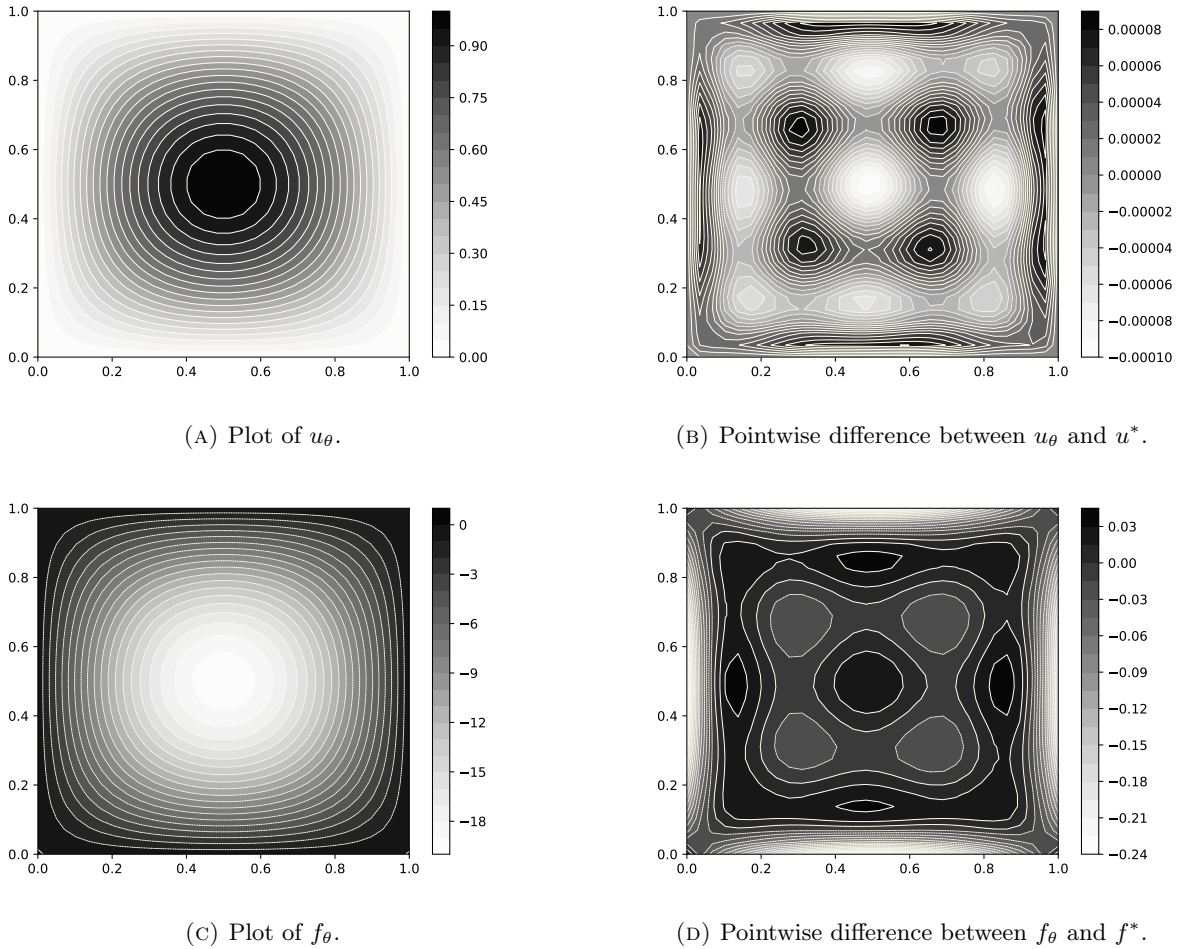


FIGURE 10. Example 5.3. Plots of  $u_\theta$  and  $f_\theta$  (left), and  $u_\theta - u^*$  and  $f_\theta - f^*$  (right); for  $\alpha = 10^{-4}$  and  $N = 30$ .

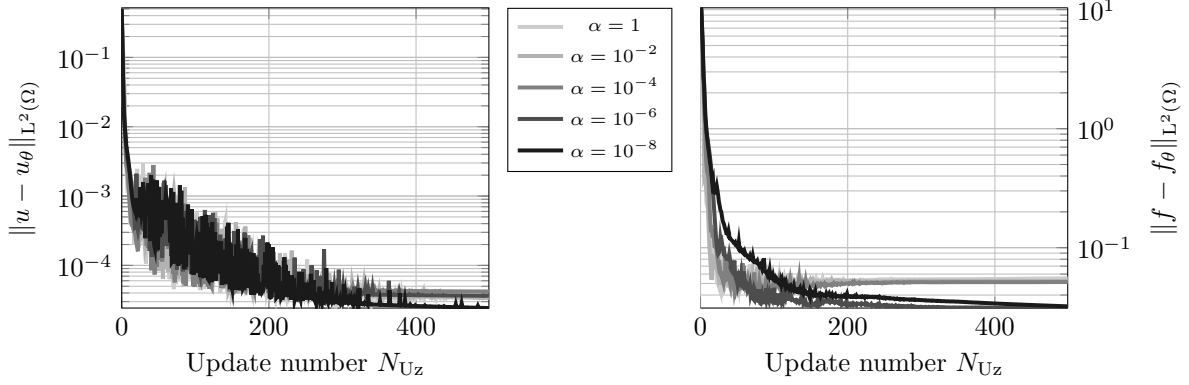


FIGURE 11. Example 5.3. Plots of the  $L^2$ -error between  $u_\theta, f_\theta \in \mathcal{V}_N$ , and  $u^*, f^* \in \mathcal{V}_N$ , from equation (5.8); for  $\alpha \in [10^{-8}, 1]$ .

## 6. NUMERICAL EXPERIMENTS: ALLEN-CAHN EQUATION

To demonstrate robustness of the methodology we consider a semi-linear PDE constraint, the Allen-Cahn equation. Let  $\epsilon > 0$  be given, we seek a  $u^* \in \widehat{\mathbf{H}} := (\mathbf{L}^6 \cap \mathbf{H}_0^1 \cap \mathbf{H}^2)(\Omega)$  and  $f^* \in \mathbf{L}^2(\Omega)$  such that

$$(6.1) \quad u^*, f^* := \arg \min_{u, f \in \widehat{\mathbf{H}} \times \mathbf{L}^2(\Omega)} \left( \frac{1}{2} \|u - \mathcal{D}\|_{\mathbf{L}^2(\Omega)}^2 + \frac{\alpha}{4} \|f\|_{\mathbf{L}^2(\Omega)}^2 + \frac{\alpha}{4} \|Au\|_{\mathbf{L}^2(\Omega)}^2 \right)$$

subject to the constraint

$$(6.2) \quad Au := -\Delta u - \frac{1}{\epsilon^2} u(1 - u^2) = f.$$

This is a challenging operator which is not guaranteed to have a unique solution.

We compute the linearisation of the operator as

$$(6.3) \quad DA\phi := -\Delta\phi - \frac{1}{\epsilon^2}(\phi + 3\phi u^2),$$

then the first-order optimality conditions are

$$(6.4) \quad \begin{aligned} \langle Au - f, \phi \rangle_{\mathbf{L}^2(\Omega)} &= 0 & \forall \phi \in \mathbf{L}^2(\Omega) \\ \langle u - \mathcal{D}, \psi \rangle_{\mathbf{L}^2(\Omega)} + \frac{\alpha}{2} \langle Au, DA\psi \rangle_{\mathbf{L}^2(\Omega)} - \langle z, DA\psi \rangle_{\mathbf{L}^2(\Omega)} &= 0 & \forall \psi \in \widehat{\mathbf{H}} \\ \langle \alpha f - z, \xi \rangle_{\mathbf{L}^2(\Omega)} &= 0 & \forall \xi \in \mathbf{L}^2(\Omega). \end{aligned}$$

**6.1. Example: Sine solution.** We choose target function  $\mathcal{D}$  such that an exact solution is given by

$$(6.5) \quad u^*(x) := \sin(\pi x), \quad f^*(x) := \sin(\pi x) \left( \pi^2 - \frac{1}{\epsilon^2} (\cos(\pi x))^2 \right).$$

For a fixed  $\epsilon$ , we observe in Figure 12 that as  $\alpha$  decreases, the pointwise error between the neural network approximation and the exact solution increases. We also observe similar behaviour when we consider the  $L^2(\Omega)$  error in Figure 13, where the rate of convergence of the control, with respect to update number, decreases as  $\alpha$  decreases. For both the pointwise error and the  $L^2(\Omega)$  error, the state is robust with respect to  $\alpha$ .

For a fixed  $\alpha$  value, we observe in Figure 14 that the neural network approximations  $u_\theta, f_\theta$  fail to converge to the solutions  $u^*, f^*$ , with respect to update number, as  $\epsilon$  decreases. This is a manifestation of the lack of uniqueness of solution to the constraint, which may be observed in Figure 15.

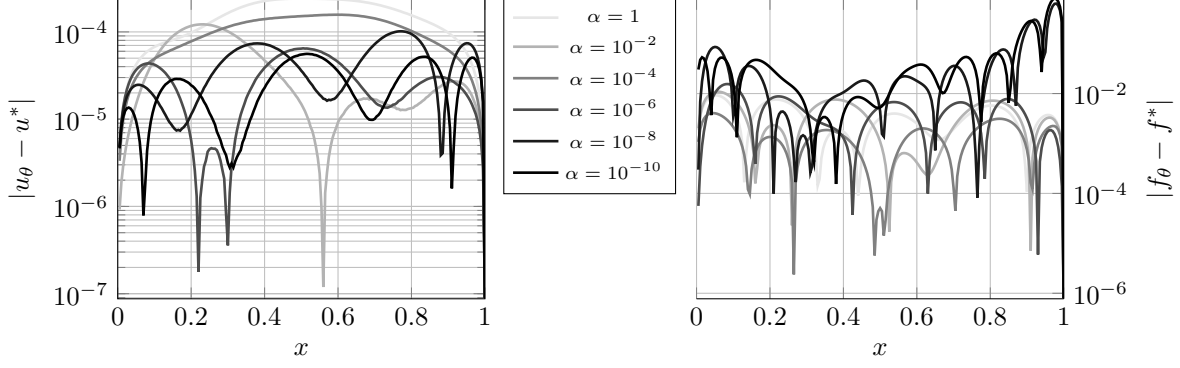


FIGURE 12. Example 6.1. Plots of the pointwise error between the neural network approximate state and control and the exact solution, for  $\epsilon = 1$  and varying  $\alpha$  values.

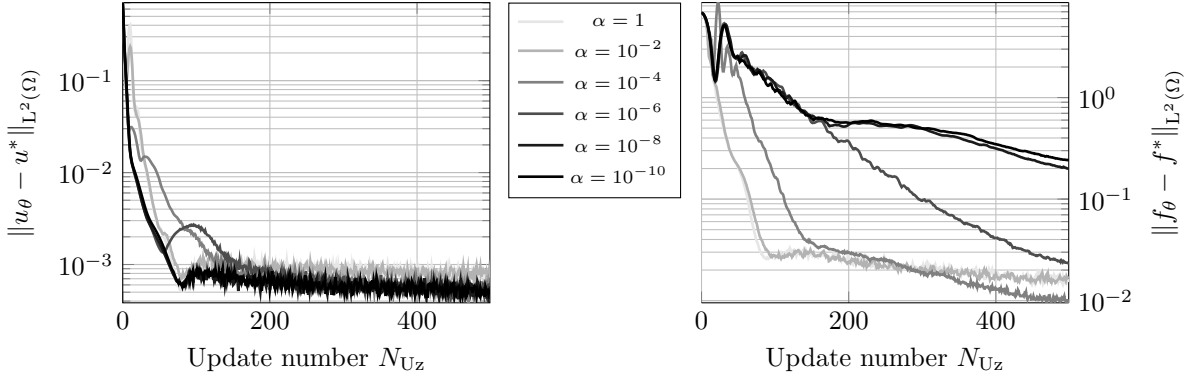


FIGURE 13. Example 6.1. Plots of the  $L^2$ -error between  $u_\theta, f_\theta$  and  $u^*, f^*$ , equation (6.5); for varying  $\alpha$  values and  $\epsilon = 1$ .

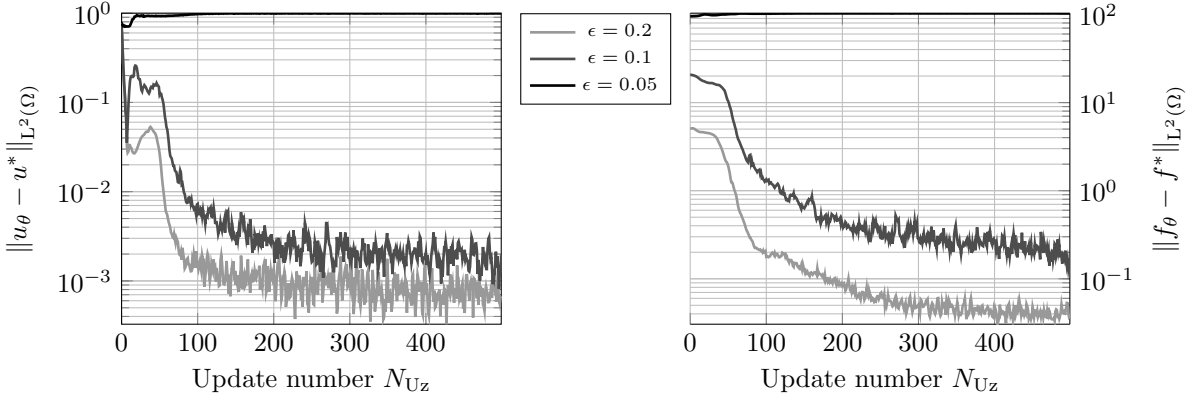


FIGURE 14. Example 6.1. Plots of the  $L^2$ -error between  $u_\theta$  and  $u^*$ , and  $f_\theta$  and  $f^*$ ; against the update number and  $\epsilon \in [0.05, 0.2]$ , for  $\alpha = 10^{-4}$ .

6.2. **Example: Step function target.** Let target function  $\mathcal{D}$  be given by

$$(6.6) \quad \mathcal{D}(x) := \begin{cases} -1 & x \in (0, \frac{1}{3}) \cup (\frac{2}{3}, 1) \\ 1 & x \in (\frac{1}{3}, \frac{2}{3}) \\ 0 & \text{otherwise.} \end{cases}$$

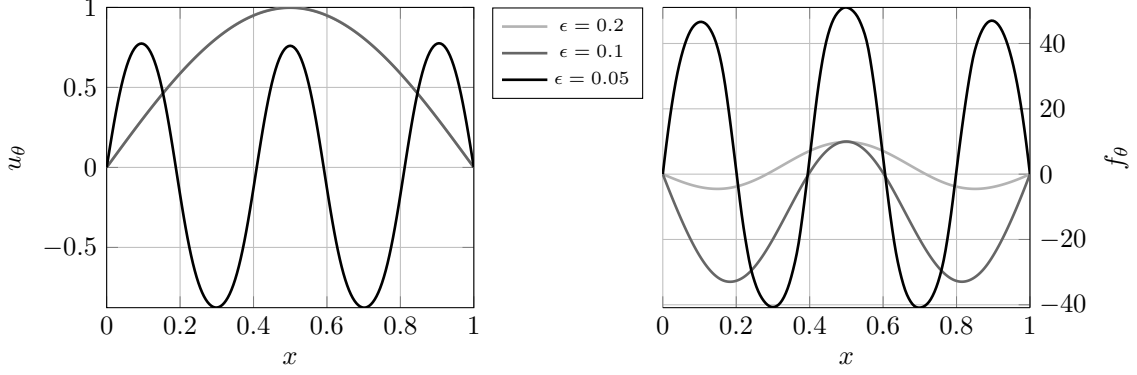


FIGURE 15. Example 6.1. Plots of the neural network approximate state and control, for  $\alpha = 10^{-4}$  and varying  $\epsilon$  values.

In the previous examples, we constructed the target such that an explicit solution was given; which we do not have in this example. In Figure 16, we observe a change in behaviour of the neural network solution as  $\alpha$  decreases. The step discontinuity in the state results in a set of large values in the control

The state converges, with respect to update number, to the target  $\mathcal{D}$  both pointwise and in  $L^2(\Omega)$ , as seen in Figure 17. Additionally, we observe that the  $L^2$ -norm of  $f_\theta$  increases proportionally to  $\alpha^{-1/2}$ .

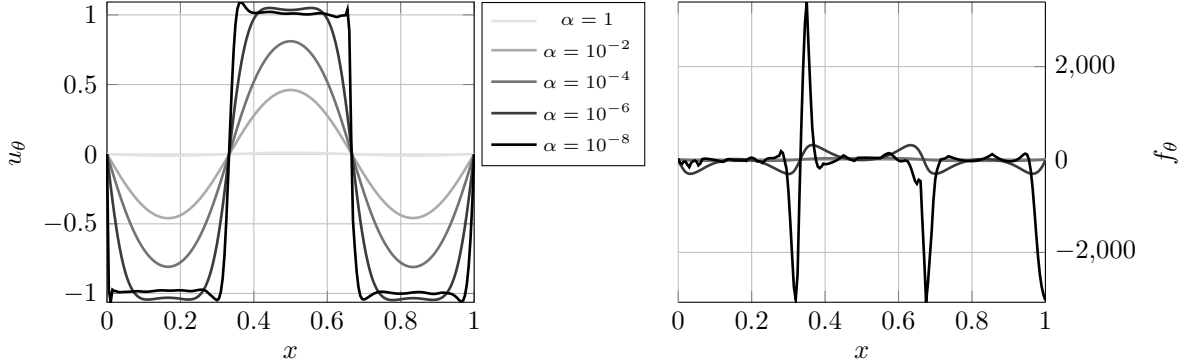


FIGURE 16. Example 6.2. Plots of the neural network approximation for the state and control, for  $\alpha \in [10^{-8}, 1]$  and  $\epsilon = 10^{-1}$ .

For a fixed  $\alpha$ , in Figure 18 we observe a transition in behaviour of the neural network approximation to the control at  $\epsilon = 0.1$ ; where the peaks and troughs flatten. A second transition in behaviour occurs when  $\epsilon = 0.05$ , where the amplitude of the state decreases and the frequency of both the state and control increases. Similar to Example 6.1, this transition in behaviour is the result of the lack of uniqueness in the constraint.

**6.3. Example: 2d Allen-Cahn equation.** In the following we consider the two-dimensional Allen-Cahn (6.2) as the PDE constraint. The two-dimensional target function  $\mathcal{D}$  is given by the normalised greyscale values of the image in Figure 19a. In Figures 19b-19c, plots of the solution  $u_\theta$  are illustrated.

## 7. PROOF OF THEOREMS 3.1 AND 3.4

**Lemma 7.1.** *Let  $u^*, f^*, z^* \in H(\Omega) \times L^2(\Omega) \times L_0^2(\Omega)$  denote the saddle point of  $L$  (2.20). Let the sequences  $\{u^k\}_{k=0}^\infty \subset H(\Omega)$ ,  $\{f^k\}_{k=0}^\infty \subset L^2(\Omega)$  and  $\{z^k\}_{k=0}^\infty \subset L_0^2(\Omega)$  be generated through the iterative method (2.21).*

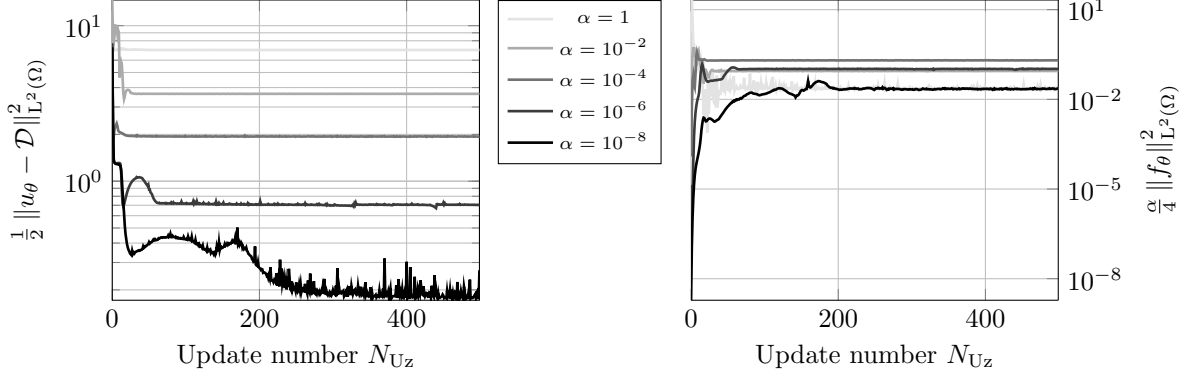


FIGURE 17. Example 6.2. Plots of the  $L^2$ -norm of the difference between the state and the target function, and the control; for  $\alpha \in [10^{-8}, 1]$  and  $\epsilon = 10^{-1}$ .

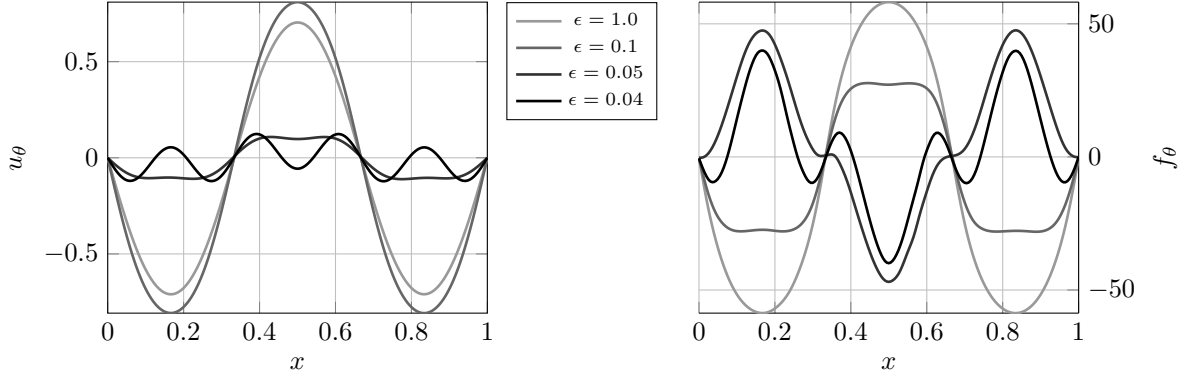


FIGURE 18. Example 6.2. Plots of the neural network approximation for the state and control, for  $\epsilon \in [0.04, 1]$  and  $\alpha = 10^{-4}$ .

Then we have

$$(7.1) \quad \langle \Delta(u^* - u^k) + f^* - f^k, z^* - z^k \rangle = \|u^* - u^k\|_{L^2(\Omega)}^2 + \frac{\alpha}{2} \|f^* - f^k\|_{L^2(\Omega)}^2 + \frac{\alpha}{2} \|\Delta(u^* - u^k)\|_{L^2(\Omega)}^2.$$

*Proof.* Integrating by parts and using the boundary conditions on  $u$  and  $z$  imply that

$$(7.2) \quad \langle \Delta(u^* - u^k), z^* - z^k \rangle + \langle f^* - f^k, z^* - z^k \rangle = \langle u^* - u^k | \Delta(z^* - z^k) \rangle_{H \times H^*} + \langle f^* - f^k, z^* - z^k \rangle.$$

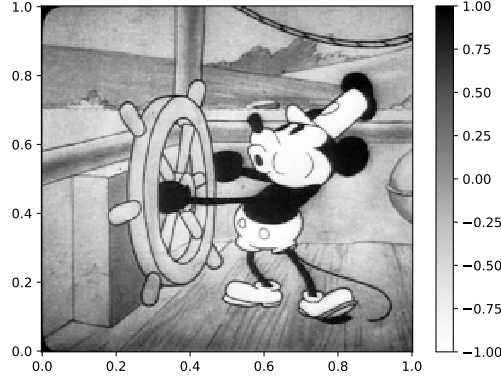
As  $u^k, f^k$  and  $u^*, f^*$  are critical points of the Lagrangian  $L$ , the first order optimality conditions are

$$(7.3) \quad \begin{aligned} \langle u^* - \mathcal{D}, \phi \rangle + \frac{\alpha}{2} \langle \Delta u^*, \Delta \phi \rangle - \langle \phi | \Delta z^* \rangle_{H \times H^*} &= 0 \quad \forall \phi \in H(\Omega), \\ \frac{\alpha}{2} \langle f^*, \psi \rangle - \langle z^*, \psi \rangle &= 0 \quad \forall \psi \in L^2(\Omega), \\ \langle u^k - \mathcal{D}, \phi \rangle + \frac{\alpha}{2} \langle \Delta u^k, \Delta \phi \rangle - \langle \phi | \Delta z^k \rangle_{H \times H^*} &= 0 \quad \forall \phi \in H(\Omega), \\ \frac{\alpha}{2} \langle f^k, \psi \rangle - \langle z^k, \psi \rangle &= 0 \quad \forall \psi \in L^2(\Omega). \end{aligned}$$

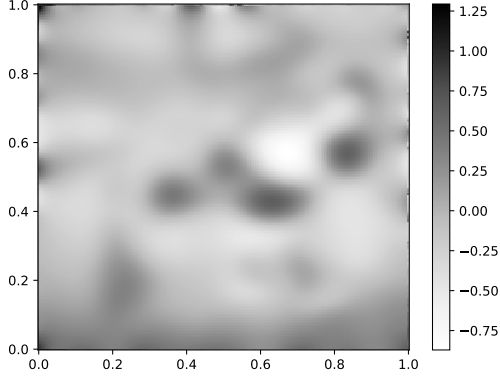
Let  $\phi := u^* - u^k$  and  $\psi := f^* - f^k$ , and consider the difference

$$(7.4) \quad \begin{aligned} \|u^k - u^*\|_{L^2(\Omega)}^2 + \frac{\alpha}{2} \|\Delta(u^k - u^*)\|_{L^2(\Omega)}^2 - \langle u^* - u^k | \Delta(z^* - z^k) \rangle_{H \times H^*} &= 0 \\ \frac{\alpha}{2} \|f^k - f^*\|_{L^2(\Omega)}^2 - \langle f^* - f^k, z^* - z^k \rangle &= 0. \end{aligned}$$

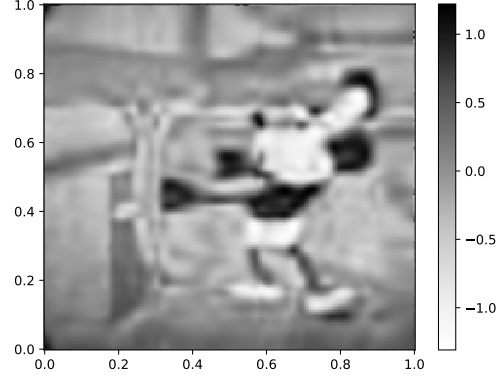
Substituting equation (7.4) into equation (7.2) we obtain our result.  $\square$



(A) Plot of  $\mathcal{D}$ .



(B) Plot of  $u_\theta$ ,  $\alpha = 10^{-6}$ ,  $\epsilon = 0.1$ .



(C) Plot of  $u_\theta$ ,  $\alpha = 10^{-10}$ ,  $\epsilon = 0.1$ .

FIGURE 19. (A) The two-dimensional target function  $\mathcal{D}$ . The still is of the public domain character Mickey Mouse, from Steamboat Willie (1928). (B)-(C) Plots of the state  $u_\theta$  for varying values of  $\alpha$  and  $\epsilon = 0.1$ .

**Lemma 7.2.** *Let  $L : \mathbf{H}(\Omega) \times \mathbf{L}^2(\Omega) \times \mathbf{L}_0^2(\Omega) \rightarrow \mathbb{R}$  denote the Lagrangian (2.17). Let  $u^*, f^*, z^* \in \mathbf{H}(\Omega) \times \mathbf{L}^2(\Omega) \times \mathbf{L}_0^2(\Omega)$  denote the saddle point of  $L$ , equation (2.20). Then*

$$(7.5) \quad z^* = z^* + \rho(\Delta u^* + f^*).$$

*Proof.* Note that  $z^*$  maximises the Lagrangian, thus

$$(7.6) \quad L(u, f, z) \leq L(u, f, z^*) \quad \forall u, f, z \in \mathbf{H}(\Omega) \times \mathbf{L}^2(\Omega) \times \mathbf{L}_0^2(\Omega).$$

Substituting the definition of the Lagrangian Now, in view of (2.17) we have

$$(7.7) \quad J(u, f) + \langle \Delta u + f, z \rangle \leq J(u, f) + \langle \Delta u + f, z^* \rangle \quad \forall u, f, z \in \mathbf{H}(\Omega) \times \mathbf{L}^2(\Omega) \times \mathbf{L}_0^2(\Omega).$$

Rearranging we obtain

$$(7.8) \quad \langle \Delta u + f, z^* - z \rangle \geq 0 \quad \forall u, f, z \in \mathbf{H}(\Omega) \times \mathbf{L}^2(\Omega) \times \mathbf{L}_0^2(\Omega).$$

Thus for  $u = u^*$  and  $f = f^*$  we have that

$$(7.9) \quad \begin{aligned} 0 &\leq \langle z^* - z^*, z^* - z \rangle + \rho \langle \Delta u^* + f^*, z^* - z \rangle \\ &= \langle z^* + \rho(\Delta u^* + f^*), z^* - z \rangle - \langle z^*, z^* - z \rangle \quad \forall z \in \mathbf{L}_0^2(\Omega), \end{aligned}$$

as required. □

**Lemma 7.3** (Elliptic Regularity [15, Theorem 4.2.2.2]). *Let  $\Omega \subset \mathbb{R}^d$  be a bounded, convex polygonal domain. For each  $f \in L^2(\Omega)$ , there exists a unique  $u \in \mathbf{H}(\Omega)$  such that*

$$(7.10) \quad \begin{aligned} -\Delta u &= f \text{ in } \Omega, \\ u &= 0 \text{ on } \partial\Omega. \end{aligned}$$

Moreover, there exists a constant  $C_{\text{reg}} > 0$  such that

$$(7.11) \quad \|u\|_{\mathbf{H}^2(\Omega)} \leq C_{\text{reg}} \|f\|_{L^2(\Omega)}.$$

**7.4. Proof of Theorem 3.1.** The proof of this result takes inspiration from [9]. Using the definition of the Uzawa update (2.21) and Lemma 7.2 we have that

$$(7.12) \quad \begin{aligned} \|z^{k+1} - z^*\|_{L^2(\Omega)}^2 &= \|(z^k - \rho(\Delta u^k + f^k)) - (z^* - \rho(\Delta u^* + f^*))\|_{L^2(\Omega)}^2, \\ &= \|(z^k - z^*) - \rho(\Delta(u^k - u^*) + (f^k - f^*))\|_{L^2(\Omega)}^2. \end{aligned}$$

Now by the definition of the norm and Lemma 7.1

$$(7.13) \quad \begin{aligned} \|z^{k+1} - z^*\|_{L^2(\Omega)}^2 &= \|z^k - z^*\|_{L^2(\Omega)}^2 + \rho^2 \|\Delta(u^k - u^*) + (f^k - f^*)\|_{L^2(\Omega)}^2 \\ &\quad - 2\rho \langle z^k - z^*, \Delta(u^k - u^*) + (f^k - f^*) \rangle, \\ &= \|z^k - z^*\|_{L^2(\Omega)}^2 + \rho^2 \|\Delta(u^k - u^*) + (f^k - f^*)\|_{L^2(\Omega)}^2 \\ &\quad - 2\rho \|u^* - u^k\|_{L^2(\Omega)}^2 - \alpha\rho \|f^* - f^k\|_{L^2(\Omega)}^2 - \alpha\rho \|\Delta(u^* - u^k)\|_{L^2(\Omega)}^2. \end{aligned}$$

The triangle and Young's inequalities imply

$$(7.14) \quad \|z^{k+1} - z^*\|_{L^2(\Omega)}^2 \leq \|z^k - z^*\|_{L^2(\Omega)}^2 + (2\rho^2 - \alpha\rho) \left( \|\Delta(u^k - u^*)\|_{L^2(\Omega)}^2 + \|(f^k - f^*)\|_{L^2(\Omega)}^2 \right).$$

If  $u^k = u^*$ ,  $f^k = f^*$  then Theorem 3.1 holds trivially. Thus without loss of generality assume that  $u^k \neq u^*$ ,  $f^k \neq f^*$  for all  $k \geq 0$ . We have that as  $\rho \leq \frac{\alpha}{2}$

$$(7.15) \quad (2\rho^2 - \alpha\rho) \left( \|\Delta(u^k - u^*)\|_{L^2(\Omega)}^2 + \|f^k - f^*\|_{L^2(\Omega)}^2 \right) < 0,$$

which implies that

$$(7.16) \quad \|z^{k+1} - z^*\|_{L^2(\Omega)}^2 < \|z^k - z^*\|_{L^2(\Omega)}^2.$$

Hence

$$(7.17) \quad \lim_{k \rightarrow \infty} \|z^k - z^*\|_{L^2(\Omega)}^2 - \|z^{k+1} - z^*\|_{L^2(\Omega)}^2 = 0.$$

Hence, rearranging (7.14), we obtain

$$(7.18) \quad (\alpha\rho - 2\rho^2) \left( \|\Delta(u^k - u^*)\|_{L^2(\Omega)}^2 + \|f^k - f^*\|_{L^2(\Omega)}^2 \right) \leq \|z^k - z^*\|_{L^2(\Omega)}^2 - \|z^{k+1} - z^*\|_{L^2(\Omega)}^2.$$

Thus applying Lemma 7.3 we have that

$$(7.19) \quad 0 \leq \frac{1}{C_{\text{reg}}^2} \|u^k - u^*\|_{\mathbf{H}^2(\Omega)}^2 + \|f^k - f^*\|_{L^2(\Omega)}^2 \leq \frac{\|z^k - z^*\|_{L^2(\Omega)}^2 - \|z^{k+1} - z^*\|_{L^2(\Omega)}^2}{\alpha\rho - 2\rho^2}.$$

Whence

$$(7.20) \quad \lim_{k \rightarrow \infty} \frac{1}{C_{\text{reg}}^2} \|u^k - u^*\|_{\mathbf{H}^2(\Omega)}^2 + \|f^k - f^*\|_{L^2(\Omega)}^2 = 0,$$

as required.

**Lemma 7.5.** *Recall the function spaces  $\mathbf{H}(\Omega, \mathbb{R}^+) \subset \mathbf{H}(\Omega)$  and  $L_0^2(\Omega, \mathbb{R}^+) \subset L_0^2(\Omega)$ , equation (3.2). Let  $L : \mathbf{H}(\Omega, \mathbb{R}^+) \times L^2(\Omega, \mathbb{R}^+) \times L_0^2(\Omega, \mathbb{R}^+) \rightarrow \mathbb{R}$  be the restricted Lagrangian (2.17). Let  $u^*, f^*, z^* \in \mathbf{H}(\Omega, \mathbb{R}^+) \times$*

$L^2(\Omega, \mathbb{R}^+) \times L_0^2(\Omega, \mathbb{R}^+)$  denote the saddle point of  $L$  (2.20). Let the sequences  $\{u^k\}_{k=0}^\infty \subset H(\Omega, \mathbb{R}^+)$ ,  $\{f^k\}_{k=0}^\infty \subset L^2(\Omega, \mathbb{R}^+)$  and  $\{z^k\}_{k=0}^\infty \subset L_0^2(\Omega, \mathbb{R}^+)$  be generated through the iterative method (2.21). Then we have

$$(7.21) \quad \begin{aligned} & \|u^k - u^*\|_{L^2(\Omega)}^2 + \frac{\alpha}{2} \|f^k - f^*\|_{L^2(\Omega)}^2 + \frac{\alpha}{2} \|\Delta(u^k - u^*)\|_{L^2(\Omega)}^2 \\ & \leq \langle u^* - u^k | \Delta(z^* - z^k) \rangle_{H \times H^*} + \langle u^* - u^k, f^* - f^k \rangle. \end{aligned}$$

*Proof.* We may use integration by parts and applying the enforced Dirichlet boundary conditions on  $H(\Omega, \mathbb{R}^+)$  and  $L_0^2(\Omega, \mathbb{R}^+)$  to deduce that

$$(7.22) \quad \langle \Delta(u^* - u^k), z^* - z^k \rangle + \langle f^* - f^k, z^* - z^k \rangle = \langle u^* - u^k | \Delta(z^* - z^k) \rangle_{H \times H^*} + \langle f^* - f^k, z^* - z^k \rangle.$$

As  $u^*, f^*, z^*$  and  $u^k, f^k, z^k$  are saddle points of their respective systems, we have by the first order optimality conditions that

$$(7.23) \quad \begin{aligned} & \langle u^* - \mathcal{D}, \phi_u - u^* \rangle + \frac{\alpha}{2} \langle \Delta u^*, \Delta(\phi_u - u^*) \rangle + \langle \phi_u - u^* | \Delta z^* \rangle_{H \times H^*} + \frac{\alpha}{2} \langle f^*, \phi_f - f^* \rangle \\ & + \langle z^*, \phi_f - f^* \rangle \geq 0 \quad \forall \phi_u, \phi_f \in H(\Omega, \mathbb{R}^+) \times L^2(\Omega, \mathbb{R}^+) \end{aligned}$$

$$(7.24) \quad \begin{aligned} & \langle u^k - \mathcal{D}, \psi_u - u^k \rangle + \frac{\alpha}{2} \langle \Delta u^k, \Delta(\psi_u - u^k) \rangle + \langle \psi_u - u^k | \Delta z^k \rangle_{H \times H^*} + \frac{\alpha}{2} \langle f^k, \psi_f - f^k \rangle \\ & + \langle z^k, \psi_f - f^k \rangle \geq 0 \quad \forall \psi_u, \psi_f \in H(\Omega, \mathbb{R}^+) \times L^2(\Omega, \mathbb{R}^+) \end{aligned}$$

Thus setting  $\phi_u = u^k$ ,  $\phi_f = f^k$ ,  $\psi_u = u^*$  and  $\psi_f = f^*$ , and considering the sum of the above equations, we have our result.  $\square$

**Lemma 7.6.** Let  $L : H(\Omega, \mathbb{R}^+) \times L^2(\Omega, \mathbb{R}^+) \times L_0^2(\Omega, \mathbb{R}^+) \rightarrow \mathbb{R}$  denote the Lagrangian (2.17). Let  $u^*, f^*, z^* \in H(\Omega, \mathbb{R}^+) \times L^2(\Omega, \mathbb{R}^+) \times L_0^2(\Omega, \mathbb{R}^+)$  denote the saddle point of  $L$ , equation (2.20). Let  $P^+ : L^2(\Omega) \rightarrow L^2(\Omega, \mathbb{R}^+)$  be the canonical projection operator, equation (3.5). Then

$$(7.25) \quad z^* = P^+(z^* + \rho(\Delta u^* + f^*)).$$

*Proof.* The proof is similar to the proof of Lemma 7.2  $\square$

**Lemma 7.7** (Variational Elliptic Regularity [15, Theorem 3.2.3.1]). Let  $\Omega \subset \mathbb{R}^d$  be a bounded, convex polygonal domain. For each  $f \in L^2(\Omega, \mathbb{R}^+)$ , there exists a unique  $u \in H(\Omega, \mathbb{R}^+)$  such that

$$(7.26) \quad \langle f + \Delta u, \phi - u \rangle \geq 0 \quad \forall \phi \in H(\Omega, \mathbb{R}^+).$$

Moreover, there exists a constant  $C_{\text{reg}} > 0$  such that

$$(7.27) \quad \|u\|_{H^2(\Omega)} \leq C_{\text{reg}} \|f\|_{L^2(\Omega)}.$$

**7.8. Proof of Theorem 3.4.** As a consequence of the definition of the Uzawa update, from Equation (3.6), and Lemma 7.6 we have that

$$(7.28) \quad \|z^{k+1} - z^*\|_{L^2(\Omega)}^2 = \|P^+(z^k - \rho(\Delta u^k + f^k)) - P^+(z^* - \rho(\Delta u^* + f^*))\|_{L^2(\Omega)}^2.$$

The positive projection operator  $P^+$  is convex thus

$$(7.29) \quad \|z^{k+1} - z^*\|_{L^2(\Omega)}^2 \leq \|P^+((z^k - \rho(\Delta u^k + f^k)) - (z^* - \rho(\Delta u^* + f^*)))\|_{L^2(\Omega)}^2.$$

Additionally, the operator satisfies  $\|P^+\phi\|_{L^2(\Omega)} \leq \|\phi\|_{L^2(\Omega)}$ , thus

$$(7.30) \quad \|z^{k+1} - z^*\|_{L^2(\Omega)}^2 \leq \|(z^k - \rho(\Delta u^k + f^k)) - (z^* - \rho(\Delta u^* + f^*))\|_{L^2(\Omega)}^2.$$

Now by the definition of the norm and Lemma 7.5

$$(7.31) \quad \begin{aligned} \|z^{k+1} - z^*\|_{L^2(\Omega)}^2 & \leq \|z^k - z^*\|_{L^2(\Omega)}^2 + \rho^2 \|\Delta(u^k - u^*) + (f^k - f^*)\|_{L^2(\Omega)}^2 \\ & \quad - 2\rho \|u^* - u^k\|_{L^2(\Omega)}^2 - \alpha\rho \|f^* - f^k\|_{L^2(\Omega)}^2 - \alpha\rho \|\Delta(u^* - u^k)\|_{L^2(\Omega)}^2. \end{aligned}$$

Applying the same methodology as §7.4, we have

$$(7.32) \quad \lim_{k \rightarrow \infty} \|z^k - z^*\|_{L^2(\Omega)}^2 - \|z^{k+1} - z^*\|_{L^2(\Omega)}^2 = 0.$$

Hence

$$(7.33) \quad \lim_{k \rightarrow \infty} \left( \|\Delta(u^k - u^*)\|_{L^2(\Omega)}^2 + \|f^k - f^*\|_{L^2(\Omega)}^2 \right) \leq \lim_{k \rightarrow \infty} \frac{\|z^k - z^*\|_{L^2(\Omega)}^2 - \|z^{k+1} - z^*\|_{L^2(\Omega)}^2}{\alpha\rho - 2\rho^2} \rightarrow 0.$$

Thus applying Lemma 7.7, we have that

$$(7.34) \quad 0 \leq \lim_{k \rightarrow \infty} \frac{1}{C_{\text{reg}}^2} \|u^k - u^*\|_{H^2(\Omega)}^2 + \|f^k - f^*\|_{L^2(\Omega)}^2 \leq 0.$$

Thus we have our result.

#### ACKNOWLEDGEMENTS

Tristan Pryer is grateful for the hospitality of ITE, Crete, where this work was initiated. Aaron Pim and Tristan Pryer received support from the EPSRC programme grant EP/W026899/1. Tristan Pryer was also supported by the Leverhulme RPG-2021-238 and EPSRC grant EP/X030067/1.

#### REFERENCES

- [1] A. Allendes, F. Fuica, and E. Otárola. “Adaptive finite element methods for sparse PDE-constrained optimization”. In: *IMA Journal of Numerical Analysis* 40.3 (2020), pp. 2106–2142.
- [2] J. Barry-Straume, A. Sarshar, A. A. Popov, and A. Sandu. “Physics-informed neural networks for PDE-constrained optimization and control”. In: *arXiv preprint arXiv:2205.03377* (2022).
- [3] D. P. Bertsekas and D. A. Castanon. “Rollout algorithms for stochastic scheduling problems”. In: *Journal of Heuristics* 5 (1999), pp. 89–108.
- [4] L. T. Biegler, O. Ghattas, M. Heinkenschloss, and B. van Bloemen Waanders. “Large-scale PDE-constrained optimization: an introduction”. In: *Large-scale PDE-constrained optimization*. Springer, 2003, pp. 3–13.
- [5] S. C. Brenner, J. Gedicke, and L.-Y. Sung. “C<sup>0</sup> Interior Penalty Methods for an Elliptic Distributed Optimal Control Problem on Nonconvex Polygonal Domains with Pointwise State Constraints”. In: *SIAM Journal on Numerical Analysis* 56.3 (2018), pp. 1758–1785.
- [6] E. Casas and K. Chrysafinos. “Analysis and Optimal Control of Some Quasilinear Parabolic Equations.” In: *Mathematical Control & Related Fields* 8 (2018).
- [7] K. Chrysafinos and D. Plaka. “Analysis and approximations of an optimal control problem for the Allen–Cahn equation”. In: *Numerische Mathematik* 155.1-2 (2023), pp. 35–82.
- [8] S. Chun and J. S. Hesthaven. “PDE constrained optimization and design of frozen mode crystals”. In: *Communications in Computational Physics* 3.4 (2008), pp. 878–898.
- [9] P. G. Ciarlet, B. Miara, and J.-M. Thomas. *Introduction to numerical linear algebra and optimisation*. Cambridge university press, 1989.
- [10] A. M. Cox, L. Hattam, A. E. Kyprianou, and T. Pryer. “A Bayesian Inverse Approach to Proton Therapy Dose Delivery Verification”. In: *arXiv preprint arXiv:2311.10769* (2023).
- [11] J. C. De los Reyes. *Numerical PDE-constrained optimization*. Springer, 2015.
- [12] S. Dolgov and M. Stoll. “Low-rank solution to an optimization problem constrained by the Navier–Stokes equations”. In: *SIAM Journal on Scientific Computing* 39.1 (2017), A255–A280.
- [13] B. Endtmayer, U. Langer, I. Neitzel, T. Wick, and W. Wollner. “Multigoal-oriented optimal control problems with nonlinear PDE constraints”. In: *Computers & Mathematics with Applications* 79.10 (2020), pp. 3001–3026.
- [14] L. C. Evans. *Partial Differential Equations*. Vol. 19. Graduate Studies in Mathematics. American Mathematical Society, 1997.
- [15] P. Grisvard. *Elliptic problems in nonsmooth domains*. SIAM, 2011.
- [16] H. Harbrecht, A. Kunoth, V. Simoncini, and K. Urban. “Optimization Problems for PDEs in Weak Space-Time Form”. In: *Oberwolfach Reports* 20.1 (2023), pp. 681–740.
- [17] D. P. Kingma and J. Ba. “Adam: A Method for Stochastic Optimization”. In: *CoRR* abs/1412.6980 (2014). URL: <https://api.semanticscholar.org/CorpusID:6628106>.

- [18] P. Kolvenbach, O. Lass, and S. Ulbrich. “An approach for robust PDE-constrained optimization with application to shape optimization of electrical engines and of dynamic elastic structures under uncertainty”. In: *Optimization and Engineering* 19 (2018), pp. 697–731.
- [19] A. Kunoth. “Wavelet-based multiresolution methods for stationary PDEs and PDE-constrained control problems”. In: *Frontiers of Numerical Analysis*. Springer, 2005, pp. 1–63.
- [20] L. Lu, R. Pestourie, W. Yao, Z. Wang, F. Verdugo, and S. G. Johnson. “Physics-informed neural networks with hard constraints for inverse design”. In: *SIAM Journal on Scientific Computing* 43.6 (2021), pp. 1105–1132.
- [21] D. Luo, T. O’Leary-Roseberry, P. Chen, and O. Ghattas. “Efficient PDE-constrained optimization under high-dimensional uncertainty using derivative-informed neural operators”. In: *arXiv preprint arXiv:2305.20053* (2023).
- [22] F. Pichi, M. Strazzullo, F. Ballarin, and G. Rozza. “Driving bifurcating parametrized nonlinear PDEs by optimal control strategies: application to Navier–Stokes equations with model order reduction”. In: *ESAIM: Mathematical Modelling and Numerical Analysis* 56.4 (2022), pp. 1361–1400.
- [23] M. Raissi, P. Perdikaris, and G. E. Karniadakis. “Physics-informed neural networks: A deep learning framework for solving forward and inverse problems involving nonlinear partial differential equations”. In: *Journal of Computational physics* 378 (2019), pp. 686–707.
- [24] T. Rees, H. S. Dollar, and A. J. Wathen. “Optimal solvers for PDE-constrained optimization”. In: *SIAM Journal on Scientific Computing* 32.1 (2010), pp. 271–298.
- [25] J. C. Roden, R. D. Mills-Williams, J. W. Pearson, and B. D. Goddard. “MultiShape: A spectral element method, with applications to dynamic density functional theory and PDE-constrained optimization”. In: *arXiv preprint arXiv:2207.05589* (2022).
- [26] J. Sirignano, J. MacArt, and K. Spiliopoulos. “PDE-constrained models with neural network terms: Optimization and global convergence”. In: *Journal of Computational Physics* 481 (2023), p. 112016.
- [27] H. Uzawa. “Iterative methods for concave programming”. In: *Studies in linear and nonlinear programming* 6 (1958), pp. 154–165.

DMAM, UNIVERSITY OF CRETE / INSTITUTE OF APPLIED AND COMPUTATIONAL MATHEMATICS, FORTH, 700 13 HERAKLION, CRETE, GREECE, AND MPS, UNIVERSITY OF SUSSEX, BRIGHTON BN1 9QH, UNITED KINGDOM  
*Email address:* C.G.Makridakis@iacm.forth.gr

AARON PIM, DEPARTMENT OF MATHEMATICAL SCIENCES, UNIVERSITY OF BATH, CLAVERTON DOWN, BATH BA2 7AY, UK.  
A.R.Pim@bath.ac.uk

TRISTAN PRYER, DEPARTMENT OF MATHEMATICAL SCIENCES, UNIVERSITY OF BATH, CLAVERTON DOWN, BATH BA2 7AY, UK.  
tmp38@bath.ac.uk